Eigenvalue-Decomposition-Precoded Ultra-Dense Non-Orthogonal Frequency-Division Multiplexing

Seichiroh Osaki, *Student Member, IEEE*, Takumi Ishihara, *Member, IEEE*, and Shinya Sugiura, *Senior Member, IEEE*

***Abstract*— This paper proposes a novel ultra-dense non-orthogonal frequency-division multiplexing (NOFDM) transmission, where subcarrier spacing is set significantly lower than that of orthogonal frequency-division multiplexing (OFDM). In order to eliminate the detrimental effects of NOFDM-specific inter-carrier interference and correlated additive noises, eigenvalue-decomposition-aided precoding is conceived. The classical capacity formula is extended to one supporting our precoded NOFDM scheme. Optimal power allocation (PA) is developed in order to maximize the derived capacity of the proposed scheme. Furthermore, truncated PA is developed to combat the limitations due to significantly low eigenvalues, which are specifically imposed by the proposed ultra-dense NOFDM. Through analytical and numerical results, we demonstrate that the proposed NOFDM schemes with optimal and truncated PA outperform the conventional NOFDM and the classical OFDM schemes.**

***Index Terms*— Capacity, eigenvalue decomposition, faster-than-Nyquist signaling, information rate, information-theoretic analysis, non-orthogonal frequency-division multiplexing, orthogonal frequency-division multiplexing, power allocation, spectrally efficient frequency-division multiplexing, truncation.**

I. Introduction

NON-ORTHOGONAL resource allocation in the time [2], frequency [3], [4], and spatial (power) domains [5] has the potential of significantly improving the performance attainable by the orthogonal resource allocation counterparts. In general, the benefits of non-orthogonal resource allocation are achieved at the cost of additional detection complexity, induced by the presence of inter-channel interference.

Manuscript received February 28, 2020; revised May 18, 2020 and July 10, 2020; accepted August 24, 2020. Date of publication September 2, 2020; date of current version December 10, 2020. This work was supported in part by the Japan Society for the Promotion of Science (JSPS) KAKENHI under Grant 16KK0120, Grant 17H03259, and Grant 17K18871 and in part by the Japan Science and Technology Agency (JST) Precursory Research for Embryonic Science and Technology (PRESTO) under Grant JPMJPR1933. This article was presented in part at the 2020 IEEE Vehicular Technology Conference (VTC2020-Fall). The associate editor coordinating the review of this article and approving it for publication was O. Ozel. *(Corresponding author: Shinya Sugiura.)*

Seichiroh Osaki is with the Department of Computer and Information Sciences, Tokyo University of Agriculture and Technology, Tokyo 184-8588, Japan.

Takumi Ishihara is with the Institute of Industrial Science, The University of Tokyo, Tokyo 153-8505, Japan.

Shinya Sugiura is with the Institute of Industrial Science, The University of Tokyo, Tokyo 153-8505, Japan, and also with the PRESTO, Japan Science and Technology Agency (JST), Kawaguchi 332-0012, Japan (e-mail: sugiura@iis.u-tokyo.ac.jp).

Color versions of one or more of the figures in this article are available online at https://ieeexplore.ieee.org.

Digital Object Identifier 10.1109/TWC.2020.3019664

Non-orthogonal resource allocation in the frequency domain has been developed in several different contexts, such as non-orthogonal frequency-division multiplexing (NOFDM) [6], [7], generalized frequency-division multiplexing (GFDM) [8], [9], and spectrally efficient frequency-division multiplexing (SEFDM) [10–15], in contrast to the classical orthogonal frequency-division multiplexing (OFDM) counterpart [16].[1] In NOFDM, by allowing the introduction of inter-carrier interference (ICI) between non-orthogonally overlapped subcarriers, more flexible resource allocation becomes realistic relative to in OFDM. Furthermore, in addition to the scenario of microwave communications, NOFDM was experimentally investigated in the context of the optical fiber communications [17], [18], the visible light communications [19], and the E-band wireless transmission [20]. In [21], the precoded NOFDM scheme was presented for decoupling ICI effects between substreams, while any power allocation (PA) onto a substream is not incorporated. However, information-theoretic analysis of the explicit merits attained by NOFDM has not been well investigated. The only exception is that in [22], where the potential capacity gain of NOFDM was shown in a scenario of NOFDM transmission without any precoding and PA.

Time-domain non-orthogonal resource allocation has been developed as faster-than-Nyquist (FTN) signaling. FTN signaling was first introduced in the early 1970s [23], [24] and relies on the transmission of non-orthogonal pulses whose interval is shorter than that defined by the inter-symbol interference (ISI)-free Nyquist criterion. Additionally, the combination of time- and frequency-domain resource allocation was also developed as multi-carrier FTN (MC-FTN) signaling [25], [26] and FTN-NOFDM [27]. The theoretical information rate of conventional FTN signaling was analyzed in [28], [29], where a performance gain of the FTN signaling scheme over the Nyquist-based counterpart was shown to be attained owing to the exploitation of the excessive bandwidth under the assumption of the use of a root raised cosine (RRC) shaping filter. However, the benefits of FTN signaling over the Nyquist counterpart were not clarified in the absence of the excess bandwidth.

Most recently, in [30], singular value decomposition (SVD)-precoded FTN signaling with optimal and truncated PA was proposed, where the classical Shannon limit is extended to one

[1] In this paper, we refer to the family of the non-orthogonal resource allocation techniques in the frequency domain as NOFDM.

supporting non-orthogonal symbol transmissions in the time domain. However, in general, the unprecoded and precoded FTN signaling schemes typically assume block transmissions, and rate loss induced due to inter-block interference (IBI) is unavoidable. However, in most previous studies, the benefits of FTN signaling were verified by ignoring the IBI effects.

Against this background, the novel contributions of this paper are as follows.

- Motivated by the recent concept of SVD-precoded FTN signaling [30], we propose a precoded ultra-dense NOFDM transmission, where the subcarrier spacing is set lower than that of OFDM. Information symbols, modulated onto non-orthogonal subcarriers, are precoded with eigenvalue decomposition (EVD) as well as linear PA.
- The classical capacity formula is generalized to support the proposed NOFDM, based on an ICI-free equivalent system model of NOFDM aided by EVD. The PA coefficient for each NOFDM subcarrier is optimized to maximize the derived capacity, with the aid of the Lagrange multiplier method.
- In order to combat the limitations imposed by the significantly low eigenvalues of the proposed scheme with optimal PA, we introduce the concept of truncated PA. This enables us to operate the proposed scheme in an ultra-dense NOFDM scenario, where the subcarrier spacing is ultimately low.
- Our analytical and numerical results demonstrate that the proposed precoded NOFDM scheme with optimal and truncated PA outperforms the conventional NOFDM and the classical OFDM counterparts, without imposing any substantial bandwidth broadening.

The remainder of this paper is organized as follows. In Section II, we provide the system model of the general NOFDM scheme, and in Section III, we propose our EVD-precoded NOFDM architecture. In Section IV, the capacity of the proposed NOFDM scheme is derived as an extension of the classical OFDM limit. In Section V, truncated PA of the proposed NOFDM scheme is introduced. Furthermore, in Section VI, we evaluate the power spectral density (PSD) and the peak-to-power average ratio (PAPR), while in Section VII, the numerical BER results of the channel-encoded near-capacity NOFDM scheme are provided. Finally, we conclude this paper in Section VIII.

II. System Model

In this section, we introduce the general system model of the precoded NOFDM architecture. Then, we review the conventional EVD-precoded NOFDM that does not rely on PA [21], and the associated capacity is formulated.

A. System Model of Precoded NOFDM

At the NOFDM transmitter, information bits are modulated onto N complex-valued symbols $\mathbf{s}_l = [s_{l,0}, \cdots, s_{l,N-1}]^T \in \mathbb{C}^N$, where l is the frame index, and N is the number of subcarriers. The power constraint of $\mathbb{E}[\mathbf{s}_l^H \mathbf{s}_l] = N$ is imposed on $\mathbf{s}_l$, where $\mathbb{E}[\cdot]$ represents the expectation operation. Then, the modulated symbol block $\mathbf{s}_l$ is linearly precoded by a complex-valued matrix $\mathbf{F} \in \mathbb{C}^{N \times N}$, in order to obtain the precoded symbol block of

$$\mathbf{x}_l = [x_{l,0}, x_{l,1}, \cdots, x_{l,N-1}]^T \in \mathbb{C}^N \quad (1)$$
$$= \mathbf{F}\mathbf{s}_l. \quad (2)$$

The precoding matrix $\mathbf{F}$ is designed for maintaining the power constraint of $\mathbb{E}[\mathbf{x}_l^H \mathbf{x}_l] = N$. Then, the precoded symbols $\mathbf{x}_l$ are multiplied by non-orthogonal subcarriers in the lth NOFDM frame, which are placed at closer spacing than the OFDM counterpart. More specifically, given T is the frame duration, the subcarrier spacing of NOFDM is expressed as $\Delta f = \alpha/T$, where α $(0 < \alpha \leq 1)$ is a compression factor.

The modulated NOFDM signals in the time-domain are represented by [31]

$$x(t) = \sqrt{\alpha E_0} \sum_{l=-\infty}^{\infty} \sum_{n=0}^{N-1} x_{l,n} g(t - lT) e^{j2\pi n \Delta f (t - lT)}, \quad (3)$$

where $g(t) \in \mathbb{R}$ is the impulse response of a shaping filter. In the proposed scheme, an RRC shaping filter with a roll-off factor $\beta \in \mathbb{R}$ is employed for $g(t)$, similar to filter bank multicarrier transmission [32], where each subcarrier, rather than the whole bandwidth, is bandlimited by an RRC shaping filter. Note that a rectangular pulse is used for $g(t)$ in the conventional OFDM. As shown in (3), the signal power decreases, upon decreasing the compression factor α. Furthermore, $E_0 \in \mathbb{R}$ is the transmit energy per subcarrier in the equivalent OFDM transmitter.

For the sake of simplicity, we consider the scenario of a single-frame transmission, and hence let us denote ($s_{l,n}$, $\mathbf{s}_l$, $x_{l,n}$, $\mathbf{x}_l$) as (s_n, $\mathbf{s}$, x_n, $\mathbf{x}$) in the rest of this paper. The coefficient $\sqrt{\alpha}$ (≤ 1) in (3) is added to normalize the transmit power of each NOFDM frame per unit bandwidth $\mathbb{E}\left[|x(t)|^2\right]$. Note that the special case of $\mathbf{F} = \mathbf{I}$ corresponds to the unprecoded NOFDM scheme, where $\mathbf{I} \in \mathbb{C}^{N \times N}$ is the identity matrix.

When considering a specific available bandwidth, the relationship between the number of subcarriers of NOFDM and that of OFDM N_{OFDM} is given by

$$N = \left\lfloor \frac{N_{\mathrm{OFDM}} - 1}{\alpha} \right\rfloor + 1. \quad (4)$$

If the available bandwidth is sufficiently wide, i.e., $N_{\mathrm{OFDM}} \gg 1$, N is approximated as

$$N \simeq \frac{N_{\mathrm{OFDM}}}{\alpha}. \quad (5)$$

Under the assumption of an additive white Gaussian noise (AWGN) channel, the received signals are represented by

$$r(t) = x(t) + n(t) \in \mathbb{R}, \quad (6)$$

where $n(t)$ is a complex-valued AWGN with zero mean and a noise variance of N_0. The received signals are first passed through a matched filter $g^*(-t)$, and then the filtered outputs are projected onto the NOFDM subcarriers. More specifically, the received sample corresponding to the ith subcarrier is given by

$$y_i = \int_{-\infty}^{\infty} r(t) g^*(-t) e^{-j\ 2\pi i \Delta f t} dt \in \mathbb{C}, \tag{7}$$

which also has the block representation

$$\begin{aligned} \mathbf{y} &= [y_0, y_1, \cdots, y_{N-1}]^T \in \mathbb{C}^N && (8)\\ &= \sqrt{\alpha E_0}\mathbf{H}\mathbf{x} + \boldsymbol{\eta}, && (9)\\ &= \sqrt{\alpha E_0}\mathbf{H}\mathbf{F}\mathbf{s} + \boldsymbol{\eta}, && (10)\end{aligned}$$

where the matrix $\mathbf{H} \in \mathbb{C}^{N\times N}$ represents the effects of ICI, and its ath-row and bth-column element is denoted by [22]

$$h_{a,b} = \int_{-\infty}^{\infty} g(t) g^*(-t) e^{j2\pi(b-a)\Delta f t} dt. \tag{11}$$

Note that for a finite number of subcarriers N, the ICI matrix $\mathbf{H}$ is positive semidefinite, hence having N non-zero eigenvalues. Furthermore, $\boldsymbol{\eta} = [\eta_0, \eta_1, \cdots, \eta_{N-1}]^T$ are the correlated noises, each formulated by

$$\eta_i = \int_{-\infty}^{\infty} n(t) g^*(-t) e^{-j\ 2\pi i \Delta f t} dt. \tag{12}$$

Here, the correlation matrix of the noises is calculated by

$$\mathbb{E}[\boldsymbol{\eta}\boldsymbol{\eta}^H] = N_0 \mathbf{H}. \tag{13}$$

Note that only in the NOFDM case with $\alpha = 1$ and a rectangular pulse, corresponding to the classic OFDM, the ICI matrix $\mathbf{H}$ becomes the identity matrix $\mathbf{I}$, owing to the orthogonality of subcarriers, and hence the noises $\boldsymbol{\eta}$ are uncorrelated. However, in general, NOFDM with $\alpha < 1$ suffers from the effects of correlated noises, due to the non-diagonal ICI matrix $\mathbf{H}$.

B. Conventional EVD-Precoded NOFDM

We review the conventional EVD-precoded NOFDM scheme [21]. Since $\mathbf{H}$ is a Toeplitz and Hermitian matrix, the ICI matrix $\mathbf{H}$ is diagonalized with the aid of EVD as follows:

$$\mathbf{H} = \mathbf{U}\boldsymbol{\Lambda}\mathbf{U}^T, \tag{14}$$

where $\mathbf{U} \in \mathbb{R}^{N\times N}$ is a real-valued unitary matrix satisfying the relationship $\mathbf{U}\mathbf{U}^T = \mathbf{U}^T\mathbf{U} = \mathbf{I}$, and $\boldsymbol{\Lambda} = \text{diag}\{\lambda_0, \lambda_1, \cdots, \lambda_{N-1}\} \in \mathbb{R}^{N\times N}$ is a diagonal matrix that contains N non-zero eigenvalues λ_i $(i = 0, \cdots, N-1)$, arranged in ascending order. Therefore, from (10) and (14), the received sample block is expressed as

$$\mathbf{y} = \sqrt{\alpha E_0}\mathbf{U}\boldsymbol{\Lambda}\mathbf{U}^T\mathbf{F}\mathbf{s} + \boldsymbol{\eta}. \tag{15}$$

Then, by setting $\mathbf{F} = \mathbf{U}$ at the transmitter, (15) is simplified to

$$\mathbf{y} = \sqrt{\alpha E_0}\mathbf{U}\boldsymbol{\Lambda}\mathbf{s} + \boldsymbol{\eta}. \tag{16}$$

Moreover, by multiplying the weights $\mathbf{U}^T$ by the received sample block $\mathbf{y}$, we arrive at

$$\begin{aligned} \mathbf{y}_\text{d} &= [y_{\text{d},0}, \cdots, y_{\text{d},N-1}]^T \in \mathbb{C}^N && (17)\\ &= \mathbf{U}^T\mathbf{y} && (18)\\ &= \sqrt{\alpha E_0}\boldsymbol{\Lambda}\mathbf{s} + \boldsymbol{\eta}_\text{u}, && (19)\end{aligned}$$

where $\boldsymbol{\eta}_\text{u} = [\eta_{\text{u},0}, \cdots, \eta_{\text{u},N-1}]^T = \mathbf{U}^T\boldsymbol{\eta}$. Since the correlation matrix of $\boldsymbol{\eta}_\text{u}$ is given by

$$\begin{aligned} \mathbb{E}\left[\boldsymbol{\eta}_\text{u}\boldsymbol{\eta}_u^H\right] &= \mathbf{U}^T\mathbb{E}\left[\boldsymbol{\eta}\boldsymbol{\eta}^H\right]\mathbf{U} && (20)\\ &= N_0\mathbf{U}^T\mathbf{H}\mathbf{U} && (21)\\ &= N_0\boldsymbol{\Lambda}, && (22)\end{aligned}$$

$\boldsymbol{\eta}_\text{u}$ are uncorrelated noises, and the variance of $\eta_{\text{u},i}$ is denoted by

$$\mathbb{E}\left[|\eta_{\text{u},i}|^2\right] = N_0\lambda_i. \tag{23}$$

In (19), since $\boldsymbol{\Lambda}$ is diagonal, the N weighted received samples $\mathbf{y}_\text{d}$ are equalized to the N ICI-free parallel substreams with uncorrelated noises as follows:

$$y_{\text{d},i} = \sqrt{\alpha E_0}\lambda_i s_i + \eta_{\text{u},i} \quad (i = 0, \cdots, N-1). \tag{24}$$

where the equivalent gain associated with the ith subchannel is represented by $\sqrt{\alpha E_0}\lambda_i$. This allows the use of maximum-likelihood (ML) detection for each substream with low complexity. Note that the calculations of the precoding matrix $\mathbf{U}$ are implemented offline in advance of NOFDM transmission, since $\mathbf{H}$ is determined uniquely by the parameters of α, β, and N.

A further note regarding (19) is that the equivalent channel gain of the ith substream is λ_i. Hence, substream-wise rate adaptation is typically needed for the conventional EVD-precoded NOFDM scheme.

C. Capacity of the Conventional EVD-Precoded NOFDM Without PA

In this section, we derive the capacity of the conventional EVD-precoded NOFDM, motivated by an information-theoretic analysis conducted for precoded FTN signaling [30].[2]

Mutual information between $\mathbf{y}_\text{d}$ and $\mathbf{s}$ is given by

$$\begin{aligned} I(\mathbf{s};\mathbf{y}_\text{d}) &= h(\mathbf{y}_\text{d}) - h(\mathbf{y}_\text{d}|\mathbf{s}) && (25)\\ &= h(\mathbf{y}_\text{d}) - h(\boldsymbol{\eta}_\text{u}) && (26)\\ &\le \log_2(|\mathbf{C}_{\mathbf{y}_\text{d}}|_\text{det}) - \log_2(|N_0\boldsymbol{\Lambda}|_\text{det}) && (27)\\ &= \log_2\left(\frac{|\mathbf{C}_{\mathbf{y}_\text{d}}|_\text{det}}{|N_0\boldsymbol{\Lambda}|_\text{det}}\right) \text{ [bits/frame]}, && (28)\end{aligned}$$

where $h(\cdot)$ denotes differential entropy. Here, we assume that the information symbols $\mathbf{s}$ and the received samples $\mathbf{y}_\text{d}$ are random variables, each obeying a Gaussian distribution [22]. Moreover, $\mathbf{C}_{\mathbf{y}_\text{d}}$ represents the covariance matrix of $\mathbf{y}_\text{d}$, which is calculated by

$$\begin{aligned} \mathbf{C}_{\mathbf{y}_\text{d}} &= \mathbb{E}\left[\mathbf{y}_\text{d}\mathbf{y}_\text{d}^H\right] && (29)\\ &= \mathbb{E}\left[\left(\sqrt{\alpha E_0}\boldsymbol{\Lambda}\mathbf{s} + \boldsymbol{\eta}_\text{u}\right)\left(\sqrt{\alpha E_0}\boldsymbol{\Lambda}\mathbf{s} + \boldsymbol{\eta}_\text{u}\right)^H\right] && (30)\\ &= \mathbb{E}\left[\alpha E_0\boldsymbol{\Lambda}\mathbf{s}\mathbf{s}^H\boldsymbol{\Lambda}\right] + \mathbb{E}\left[\boldsymbol{\eta}_\text{u}\boldsymbol{\eta}_\text{u}^H\right] && (31)\\ &= \alpha E_0\boldsymbol{\Lambda}^2 + N_0\boldsymbol{\Lambda}, && (32)\end{aligned}$$

[2]Information-theoretic analysis of the conventional EVD-precoded NOFDM scheme [21] has not been carried out before, and hence its derivation is also one of our main contributions.

where $\mathbb{E}[\mathbf{s}\mathbf{s}^H] = \mathbf{I}$. From (28) and (32), mutual information $I(\mathbf{s}; \mathbf{y}_\mathrm{d})$ is upper-bounded as

$$I(\mathbf{s}; \mathbf{y}_\mathrm{d}) \leq \log_2 \left(\frac{|\alpha E_0 \mathbf{\Lambda}^2 + N_0 \mathbf{\Lambda}|_\mathrm{det}}{|N_0 \mathbf{\Lambda}|_\mathrm{det}} \right) \tag{33}$$

$$= \log_2 \left(\left| \mathbf{I}_N + \frac{\alpha E_0}{N_0} \mathbf{\Lambda} \right|_\mathrm{det} \right) \tag{34}$$

$$= \sum_{i=0}^{N-1} \log_2 \left(1 + \frac{\alpha E_0 \lambda_i}{N_0} \right) \text{ [bits/frame]}. \tag{35}$$

By ignoring the effects of inter-frame interference ($\epsilon = 0$), the capacity of the conventional EVD-precoded NOFDM scheme, normalized by the frame duration, is formulated by

$$C_\mathrm{F,conv} = \frac{1}{T} \sum_{i=0}^{N-1} \log_2 \left(1 + \frac{\alpha E_0 \lambda_i}{N_0} \right) \text{ [bps]}. \tag{36}$$

The bandwidth consumed in the NOFDM scheme, employing the RRC filter with a roll-off factor β, is calculated by

$$W = \frac{(N-1)\alpha + 1 + \beta + \epsilon}{T} \text{ [Hz]}, \tag{37}$$

where ϵ corresponds to a bandwidth penalty imposed by time limiting [33]. Furthermore, under the assumption of $N\alpha \gg 1$, (38) is approximated by

$$W \simeq \frac{N\alpha}{T} \text{ [Hz]}. \tag{38}$$

Finally, the average capacity normalized by the bandwidth is given as follows:

$$\bar{C}_\mathrm{F,conv} = \frac{C_\mathrm{F,conv}}{W} \tag{39}$$

$$= \frac{\sum_{i=0}^{N-1} \log_2 \left(1 + \frac{\alpha E_0 \lambda_i}{N_0} \right)}{(N-1)\alpha + 1 + \beta + \epsilon} \text{ [bps/Hz]}. \tag{40}$$

For $N\alpha \gg 1$, (40) is approximated by

$$\bar{C}_\mathrm{F,conv} \simeq \frac{1}{N\alpha} \sum_{i=0}^{N-1} \log_2 \left(1 + \frac{\alpha E_0 \lambda_i}{N_0} \right) \text{ [bps/Hz]}. \tag{41}$$

As seen in (40), the capacity of the conventional EVD-precoded NOFDM depends on the eigenvalue distribution. Note that the capacity of the conventional EVD-precoded NOFDM scheme is identical to that of the conventional unprecoded NOFDM scheme, since precoding based on the unitary matrix $\mathbf{U}$ at the transmitter does not change the system model in the AWGN channel. Throughout this paper, we employed the definition of the signal-to-noise ratio (SNR) as E_0/N_0, which remains unchanged regardless of α.

III. Proposed EVD-Precoded NOFDM With Optimal PA

In this section, we introduce PA on the subcarriers in the EVD-precoded NOFDM scheme, and the PA coefficients are optimized to maximize the capacity.

A. System Model

The transceiver model of the proposed EVD-precoded NOFDM scheme with PA is depicted in Fig. 1. At the transmitter, a PA coefficient $\sqrt{q_i} \in \mathbb{R}$ is multiplied by the ith information symbol s_i. Then, power-allocated symbols $\sqrt{q_i} s_i$ $(i = 0, \cdots, N-1)$ are precoded by the unitary matrix $\mathbf{U}$, which yields

$$\mathbf{x} = \mathbf{U}\mathbf{Q}\mathbf{s}, \tag{42}$$

where

$$\mathbf{Q} = \mathrm{diag}\{\sqrt{q_0}, \sqrt{q_1}, \cdots, \sqrt{q_{N-1}}\} \in \mathbb{R}^{N \times N}. \tag{43}$$

From (15) and (42), the received sample block of the proposed EVD-precoded NOFDM with PA, transmitted over the AWGN channel, is represented by

$$\mathbf{y} = \sqrt{\alpha E_0} \mathbf{U} \mathbf{\Lambda} \mathbf{Q} \mathbf{s} + \boldsymbol{\eta}. \tag{44}$$

Then, in a similar manner to (19), the weighs of $\mathbf{U}^T$ are multiplied by the received sample block $\mathbf{y}$ as follows:

$$\mathbf{y}_\mathrm{d} = [y_{\mathrm{d},0}, \cdots, y_{\mathrm{d},N-1}]^T \in \mathbb{C}^N \tag{45}$$

$$= \mathbf{U}^T \mathbf{y} \tag{46}$$

$$= \sqrt{\alpha E_0} \mathbf{\Lambda} \mathbf{Q} \mathbf{s} + \boldsymbol{\eta}_\mathrm{u} \tag{47}$$

$$= \sqrt{\alpha E_0} \mathbf{P}^{\frac{1}{2}} \mathbf{\Lambda}^{\frac{1}{2}} \mathbf{s} + \boldsymbol{\eta}_\mathrm{u}, \tag{48}$$

where we have

$$\mathbf{P} = \mathrm{diag}\{p_0, \cdots, p_{N-1}\} \in \mathbb{R}^{N \times N}, \tag{49}$$

$$p_i = \lambda_i q_i \ (> 0). \tag{50}$$

Furthermore, the ith substream of $\mathbf{y}_\mathrm{d}$ is formulated by

$$y_{\mathrm{d},i} = \sqrt{\alpha E_0} \lambda_i \sqrt{q_i} s_i + \eta_{\mathrm{u},i}, \tag{51}$$

where the equivalent average SNR is calculated by

$$\gamma_i = \frac{\mathbb{E}\left[\left| \sqrt{\alpha E_0} \lambda_i \sqrt{q_i} s_i \right|^2 \right]}{\mathbb{E}\left[|\eta_{\mathrm{u},i}|^2 \right]} \tag{52}$$

$$= \frac{\alpha E_0 \lambda_i q_i}{N_0} \tag{53}$$

$$= \frac{\alpha E_0 p_i}{N_0}. \tag{54}$$

Hence, the equivalent energy allocated to the ith substream (subcarrier) in our optimal PA is $\alpha E_0 p_i$, rather than $\alpha E_0 q_i$.

B. Derivation of Optimal PA Coefficients

We derive the optimal PA matrix $\mathbf{Q}$ of the proposed scheme by maximizing the capacity with the aid of the Lagrange multiplier method. Since the additive noises $\boldsymbol{\eta}_\mathrm{u}$ in (48) are uncorrelated, mutual information of the proposed scheme is upper-bounded by [30]

$$I(\mathbf{s}; \mathbf{y}_\mathrm{d}) \leq \sum_{i=0}^{N-1} \log_2 \left(1 + \frac{\alpha E_0 \lambda_i q_i}{N_0} \right) \text{ [bits/frame]}. \tag{55}$$

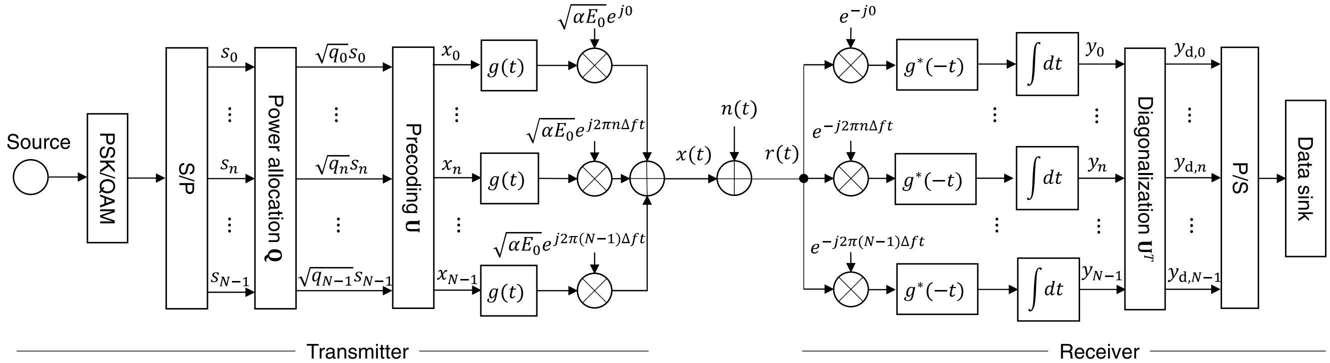

Fig. 1. Transceiver model of the proposed EVD-precoded NOFDM scheme with PA.

The transmit energy per frame in the conventional EVD-precoded NOFDM scheme without PA is given by

$$\begin{aligned} E_N &= \mathbb{E}\left[\int_{-\infty}^{\infty} |x(t)|^2 dt\right] &(56)\\ &= \alpha E_0 \mathbb{E}\left[\mathbf{x}^H \mathbf{H} \mathbf{x}\right] &(57)\\ &= \alpha E_0 \mathbb{E}\left[\mathbf{s}^H \boldsymbol{\Lambda} \mathbf{s}\right] &(58)\\ &= \alpha E_0 \sum_{i=0}^{N-1} \lambda_i \mathbb{E}\left[|s_i|^2\right] &(59)\\ &= \alpha E_0 N, &(60)\end{aligned}$$

where $\sum_{i=0}^{N-1}\lambda_i = \mathrm{trace}\{\mathbf{H}\} = N$ since each diagonal element of $\mathbf{H}$ is unity. Furthermore, the transmit energy per frame in the proposed scheme is calculated by

$$\begin{aligned} \bar{E}_N &= \mathbb{E}\left[\int_{-\infty}^{\infty} |x(t)|^2 dt\right] &(61)\\ &= \alpha E_0 \mathbb{E}\left[\mathbf{s}^H \mathbf{Q} \mathbf{U}^T \mathbf{H} \mathbf{U} \mathbf{Q} \mathbf{s}\right] &(62)\\ &= \alpha E_0 \mathbb{E}\left[\mathbf{s}^H \mathbf{Q} \boldsymbol{\Lambda} \mathbf{Q} \mathbf{s}\right] &(63)\\ &= \alpha E_0 \sum_{i=0}^{N-1} \lambda_i q_i \mathbb{E}\left[|s_i|^2\right] &(64)\\ &= \alpha E_0 \sum_{i=0}^{N-1} \lambda_i q_i. &(65)\end{aligned}$$

Note that the proposed EVD-precoded NOFDM scheme with PA subsumes the conventional EVD-precoded NOFDM scheme in its special case with the parameters of $q_0 = \cdots = q_{N-1} = 1$, i.e., $\mathbf{Q} = \mathbf{I}$. Naturally, the total transmit energy has to be unaffected by the presence or absence of PA. Hence, in order to maintain the equal transmit energy in the two schemes, we arrive at the following constraint:

$$\begin{aligned} \bar{E}_N &= E_N &(66)\\ \Leftrightarrow &\sum_{i=0}^{N-1} \lambda_i q_i = N. &(67)\end{aligned}$$

Next, in order to obtain the optimal q_i values, mutual information of (55) is maximized with respect to q_i under the energy constraint of (67). Let us consider the following Lagrange function:

$$J = \sum_{i=0}^{N-1} \log_2\left(1 + \frac{\alpha E_0 \lambda_i q_i}{N_0}\right) - \xi\left(\sum_{i=0}^{N-1} \lambda_i q_i - N\right), \quad (68)$$

where ξ is the Lagrange multiplier. Here, to maximize J with respect to q_i, we consider

$$\frac{\partial J}{\partial q_i} = 0, \text{ subject to } q_i \geq 0, \quad (69)$$

yielding

$$q_i = \frac{1}{\alpha \lambda_i E_0}\left(\frac{\alpha E_0}{(\ln 2)\xi} - N_0\right). \quad (70)$$

By substituting (70) into (67), we have

$$\xi = \frac{1}{(\ln 2)\left(1 + \frac{N_0}{\alpha E_0}\right)}. \quad (71)$$

Finally, by substituting (71) into (70), we obtain

$$q_i = \frac{1}{\lambda_i}, \quad (72)$$

which corresponds to $p_0 = \cdots = p_{N-1} = 1$. Note that (72) satisfies the condition of $q_i \geq 0$ in (69), since $\lambda_i > 0$ is guaranteed. Hence, with the proposed scheme, it is ensured that each substream encounters an identical equivalent SNR of $\gamma_0 = \cdots = \gamma_{N-1} = \alpha E_0/N_0$ in (54). Note that our optical PA solution is different from the well-known water-filling solution, which was developed for PA of OFDM transmission experiencing the frequency-selective fading channel [33]. In the water-filling solution of OFDM, higher power and data rate is assigned over the channels having higher SNRs. Furthermore, while a cut-off value exists for water-filling of OFDM, it does not in the proposed optimal PA solution. These are mainly induced from the difference of the energy constraints between the proposed NOFDM scheme in the AWGN channel and the conventional OFDM scheme in the frequency-selective channel.

C. Capacity of the Proposed Scheme

The capacity of the proposed scheme is maximized by substituting (72) into (55), which is formulated by

$$\begin{aligned} I(\mathbf{s}; \mathbf{y}_{\mathrm{d}}) &\leq \sum_{i=0}^{N-1} \log_2\left(1 + \frac{\alpha E_0}{N_0}\right) &(73)\\ &= N \log_2\left(1 + \frac{\alpha E_0}{N_0}\right) \text{[bits/frame]}. &(74)\end{aligned}$$

Also, the capacity normalized by the frame duration is given by

$$C_{\mathrm{F,opt}} = \frac{1}{T} I(\mathbf{s}; \mathbf{y}_{\mathrm{d}}) \tag{75}$$

$$= \frac{N}{T} \log_2 \left(1 + \frac{\alpha E_0}{N_0}\right) \text{[bps]}. \tag{76}$$

The capacity normalized by the bandwidth W is given by

$$\bar{C}_{\mathrm{F,opt}} = \frac{C_{\mathrm{F,opt}}}{W} \tag{77}$$

$$= \frac{N \log_2 \left(1 + \frac{\alpha E_0}{N_0}\right)}{(N-1)\alpha + 1 + \beta + \epsilon} \text{ [bps/Hz]}. \tag{78}$$

Moreover, under the assumption of $N\alpha \gg 1$, (78) is simplified to

$$\bar{C}_{\mathrm{F,opt}} = \frac{1}{\alpha} \log_2 \left(1 + \frac{\alpha E_0}{N_0}\right) \text{ [bps/Hz]}. \tag{79}$$

As formulated in (78), the capacity of the proposed scheme with optimal PA is given in closed form and does not include the eigenvalues λ_i, owing to the relationship of (72). Additionally, in the OFDM case with $\alpha = 1$ and a rectangular pulse, (78) corresponds to the classical Shannon capacity in the AWGN channel.[3] More specifically, in (79), the proposed NOFDM suffers from the power penalty of α in terms of the SNR E_0/N_0, in comparison to the OFDM counterpart, whose effects increased upon decreasing the compression factor α. However, owing to the explicit benefits of the NOFDM scheme's bandwidth compression, shown as the multiplication of $1/\alpha$, the resultant capacity $\bar{C}_{\mathrm{F,opt}}$ increases upon decreasing the α value as demonstrated in Section IV.

Moreover, we formulate the capacity in the limit of $\alpha \to 0$, similar to [30]. More specifically, by applying l'Hôpital's rule [34] to (79), we arrive at

$$\lim_{\alpha \to 0} \bar{C}_{\mathrm{F,opt}} = \lim_{\alpha \to 0} \frac{\frac{\partial}{\partial \alpha} \log_2 \left(1 + \frac{\alpha E_0}{N_0}\right)}{\frac{\partial}{\partial \alpha} \alpha} \tag{80}$$

$$= \lim_{\alpha \to 0} \frac{\frac{E_0}{N_0}}{(\ln 2)\left(1 + \frac{\alpha E_0}{N_0}\right)} \tag{81}$$

$$= \frac{1}{\ln 2} \cdot \frac{E_0}{N_0} \text{ [bps/Hz]}. \tag{82}$$

This implies that even if the compression factor is set infinitesimally low, the associated capacity is bounded by (82).

IV. Analytical Performance Results

This section presents the analytical results of the proposed EVD-precoded NOFDM scheme with optimal PA, which is compared with the conventional EVD-precoded NOFDM without PA and the classical OFDM. Here, the derived capacities of (40) and (78) are used for the evaluations.

Figs. 2(a) and 2(b) show the capacities of the conventional EVD-precoded NOFDM scheme without PA and the proposed EVD-precoded NOFDM scheme with optimal PA, respectively, each employing the RRC shaping filter with the roll-off factor of $\beta = 0.22$. The compression factor was given by $\alpha = 1.0, 0.5, 0.2, 0.1, 0.05$, and 0.01. The frame duration and the energy factor were set to $T = 1$ and $E_0 = 1$, respectively. The benchmark curve associated with the classic OFDM based on a rectangular pulse was also plotted. Observe in Fig. 2(a) that the conventional EVD-precoded NOFDM scheme with $\alpha < 1$ exhibited a higher capacity than the OFDM counterpart. More specifically, upon decreasing the compression factor α, its performance gain over OFDM increased up to $\alpha = 0.1$.[4] However, a further decrease of α resulted in the increase of ratio of the number of significantly low eigenvalues over N, which will be shown in later in Fig. 3. Hence, the capacity did not substantially increase anymore. As shown in Fig. 2(b), it was found that the proposed EVD-precoded NOFDM scheme with optimal PA achieved a significantly high capacity, outperforming the conventional EVD-precoded NOFDM without PA and the OFDM. Furthermore, upon decreasing the compression factor, the capacity of the proposed scheme asymptotically approached the limit of $\alpha \to 0$ in (82). Moreover, it can also be seen that the performance advantage of the proposed NOFDM (Fig. 2(b)) over the conventional NOFDM (Fig. 2(a)) was owing to optimal PA, where the performance gap increased upon decreasing the compression factor α. To be more specific, the proposed NOFDM scheme is capable of exploiting the subchannels, which is achieved as a result of maximizing mutual information with respect to the PA factors $\mathbf{Q}$.

Since the eigenvalues λ_i are not explicitly included in (78), it is readily possible to calculate the capacity of the proposed scheme even when there are significantly low eigenvalues. However, in practice, the proposed NOFDM transmitter has to accurately calculate all N eigenvalues to generate a frame $x(t)$, based on the precoded symbols $\mathbf{x}$ in (42). More specifically, according to (72), the optimal PA coefficient is given by the inverse of the associated eigenvalue, i.e., $q_i = 1/\lambda_i$. For example, when λ_i is too small to be accurately calculated in the standard double-precision environment, the calculated eigenvalue $\hat{\lambda}_i$ tends to contain a significantly high calculation error, such as $\hat{\lambda}_i/\lambda_i \gg 1$ or $\hat{\lambda}_i/\lambda_i \ll 1$.[5] Hence, the calculated PA coefficient $\hat{q}_i = 1/\hat{\lambda}_i$ suffers from an enhanced error by several orders of magnitude. In our extensive simulations, it was found that in such a scenario, where there are significantly low eigenvalues, the average power per frame of the generated signals was far from $\bar{E}_N$, and the associated PSD was unexpectedly broadened.

[3] The capacity formula (78) of the proposed NOFDM scheme is derived motivated by that of the time-domain counterpart, i.e., the SVD-precoded FTN signaling scheme [30]. Hence, both the NOFDM and FTN schemes exhibit comparable information rates, although there is a difference in the eigenvalue distributions, as mentioned in Section IV. Note that the recent SVD-precoded FTN signaling of [30] subsumes the conventional FTN signaling scheme [29] in its special case, hence exhibiting a higher achievable performance.

[4] These results agree with those in [22], where the capacity gain of the unprecoded conventional NOFDM scheme was derived with EVD. This is because the precoding matrix $\mathbf{U}$ used at the transmitter in the conventional EVD-precoded NOFDM scheme does not change the system model for the scenario of the AWGN channel, in comparison to that of the unprecoded NOFDM scheme.

[5] A particular positive define Toeplitz matrix of arbitrary order is referred to as a *prolate matrix* [35], where the eigenvalues cluster exponentially to the limits zero. The same limitation is imposed on the recent SVD-precoded FTN signaling scheme with optimal PA in [30].

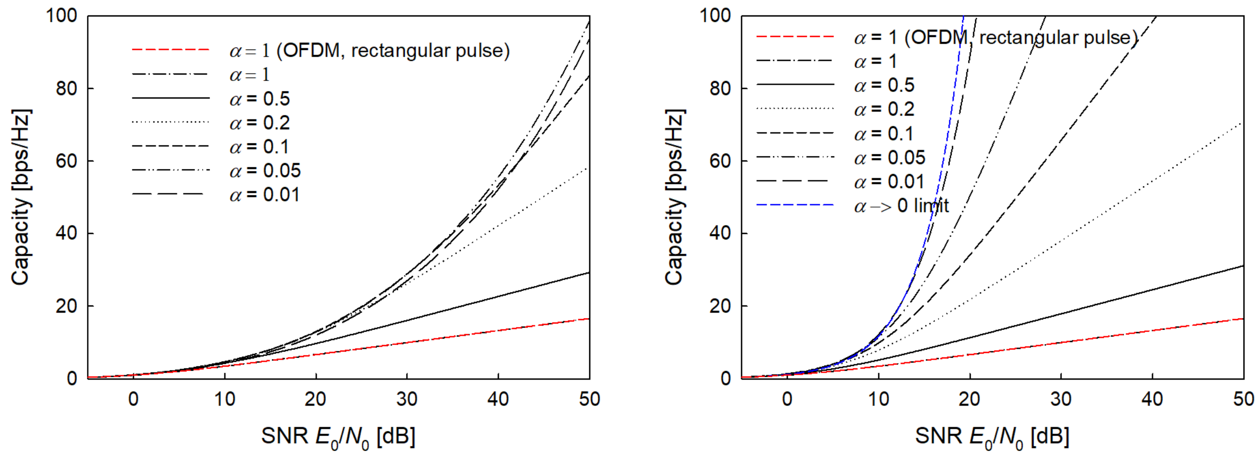

(a) Conventional EVD-precoded NOFDM

(b) Proposed EVD-precoded NOFDM

Fig. 2. Capacities of (a) the conventional EVD-precoded NOFDM scheme without PA and (b) the proposed EVD-precoded NOFDM scheme with optimal PA, each employing the RRC shaping filter with a roll-off factor of $\beta = 0.22$. The compression factor was given by $\alpha = 1.0, 0.5, 0.2, 0.1, 0.05$, and 0.01. The frame duration and the energy per subcarrier were fixed to $T = 1$ and $E_0 = 1$, respectively, while the number of the NOFDM subcarriers was fixed to $N = 1000$. The benchmark curve associated with the classic OFDM based on a rectangular pulse was also plotted.

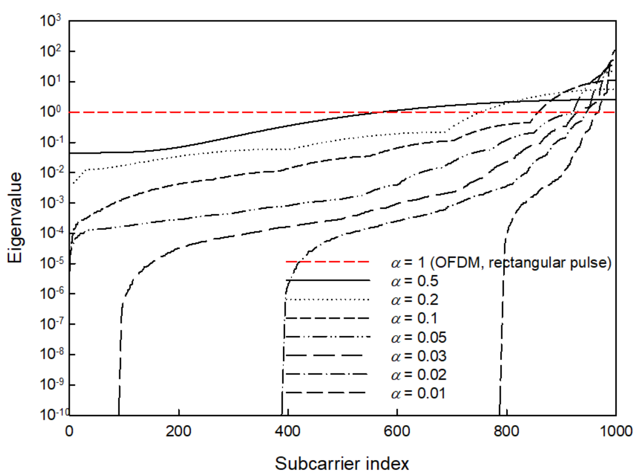

Fig. 3. Eigenvalues of the correlation matrix $\mathbf{H}$, where we considered the RRC shaping filter with $\beta = 0.22$ and the $N = 1000$ subcarriers. The compression factor was given by $\alpha = 0.5, 0.2, 0.1, 0.05, 0.03, 0.02$, and 0.01. The curve associated with the classic OFDM with a rectangular pulse was also plotted.

In order to elaborate on this issue, in Fig. 3, we show the eigenvalues of the ICI matrix $\mathbf{H}$ in the proposed scheme, where the roll-off factor of the RRC shaping filter was set to $\beta = 0.22$, and the compression factor was given by $\alpha = 0.5, 0.2, 0.1, 0.05, 0.04, 0.03, 0.02$, and 0.01. The curve associated with the classic OFDM with a rectangular pulse was also plotted, where all the eigenvalues were $\lambda_i = 1$ $(i = 0, \cdots, N-1)$. The number of subcarriers was given by $N = 1000$. Observe in Fig. 3 that some of the eigenvalues of the proposed NOFDM scheme exhibited significantly low values, such as $\lambda < 10^{-16}$, where upon decreasing the α value, the fraction of significantly low eigenvalues increased. More specifically, for $\alpha < 0.05$, some of the eigenvalues were lower than 10^{-16}. Such significantly low eigenvalues are not accurately calculated in the standard double-precision environment. This implies that accurate PA coefficients q_i cannot be calculated, since the PA coefficients include the inverse of the eigenvalues, according to (72). The use of such inaccurate PA coefficients imposes bandwidth broadening and detection errors. For $\alpha \geq 0.05$, all the eigenvalues were higher than 10^{-6}, so they were tractable in the double-precision environment.

The problem associated with significantly low eigenvalues arises in the case of the SVD-precoded FTN signaling scheme in [30], similar to the proposed EVD-precoded NOFDM scheme because both the schemes have to calculate the inverses of eigenvalues of interference matrix $\mathbf{G}$ when employing optimal PA. However, since the effects of interference in the time domain and that of the frequency domain are not identical, the resultant eigenvalue distributions are also different. More specifically, the ratio of significantly low eigenvalues in our EVD-precoded NOFDM with optimal PA is typically lower than that of the FTN signaling counterpart. For example, when considering the specific compression ratio $\alpha = 0.1$ for the NOFDM and FTN signaling schemes, employing the RRC shaping filter with $\beta = 0.22$ and the block length of $N = 1000$, the minimum eigenvalue in the NOFDM was $\min_i(\lambda_i) = 8.5 \times 10^{-5}$, while that of FTN signaling was as low as $\min_i(\lambda_i) \ll 10^{-16}$.

V. EVD-Precoded NOFDM With Truncated PA

A. System Model

In order to combat the limitations imposed by significantly low eigenvalues, we conceive the concept of truncated PA by introducing a threshold t_h for significantly low eigenvalues. More specifically, instead of (72), the truncated PA factors are given by

$$q_i = \begin{cases} \dfrac{k}{\lambda_i}, & (\lambda_i \geq t_h) \\ 0, & (\lambda_i < t_h), \end{cases} \tag{83}$$

where $k = N/M$ is a scaling factor used for satisfying the power constraint of (67), and $M(\leq N)$ is the number of activated substreams. Here, the threshold t_h is determined such that the minimum eigenvalue $\min_i(\lambda_i)$ is calculated in the standard double-precision environment. From (65), the transmit energy per frame in the proposed EVD-precoded NOFDM with truncated PA is calculated by

$$\tilde{E}_N = \alpha E_0 \sum_{i=0}^{N-1} \lambda_i q_i \tag{84}$$
$$= \alpha E_0 k M \tag{85}$$
$$= \alpha E_0 N, \tag{86}$$

which is maintained to be equal to that of the proposed scheme with optimal PA in (60).

B. Capacity of the Proposed Scheme With Truncated PA

Mutual information of the proposed EVD-precoded NOFDM with truncated PA is derived by substituting (83) into (55) as follows:

$$I(\mathbf{s};\mathbf{y}_{\mathrm{d}})_{\mathrm{trun}} \leq \sum_{i=0}^{N-1} \log_2\left(1+\frac{\alpha k E_0}{N_0}\right) \tag{87}$$
$$= M\log_2\left(1+\frac{\alpha(N/M)E_0}{N_0}\right) \text{ [bits/frame]}. \tag{88}$$

Hence, the capacity of the proposed scheme with truncated PA, normalized by the frame duration T, is given by

$$C_{\mathrm{Fw,trun}} = \frac{1}{T} I(\mathbf{s};\mathbf{y}_{\mathrm{d}})_{\mathrm{trun}} \tag{89}$$
$$= \frac{M}{T}\log_2\left(1+\frac{\alpha(N/M)E_0}{N_0}\right) \text{ [bps]}. \tag{90}$$

The capacity normalized by the bandwidth W is formulated by

$$\bar{C}_{\mathrm{Fw,trun}} = \frac{C_{\mathrm{Fw,trun}}}{W} \tag{91}$$
$$= \frac{M}{(N-1)\alpha+1+\beta+\epsilon} \cdot \log_2\left(1+\frac{\alpha(N/M)E_0}{N_0}\right) \text{ [bps/Hz]}. \tag{92}$$

Under the assumption of $\alpha N \gg 1$, the capacity normalized by the bandwidth W is simplified to

$$\bar{C}_{\mathrm{Fw,trun}} \simeq \frac{M}{N\alpha}\log_2\left(1+\frac{\alpha(N/M)E_0}{N_0}\right) \text{ [bps/Hz]}. \tag{93}$$

Here, (93) indicates that the capacity of the proposed scheme with truncated PA monotonically decreases upon decreasing the number of truncated substreams, i.e., upon increasing the thresholding value t_h. Note that since M is a function of α, it is a challenging task to derive the capacity in the limit of $\alpha \to 0$ for the proposed scheme with truncated PA, unlike in the proposed scheme with optimal PA.

Fig. 4 compares the capacities of the proposed EVD-precoded NOFDM schemes with optimal and truncated PA, where the threshold for truncation was given by $t_h = 10^{-4}$, and the roll-off factor of an RRC shaping filter was set to $\beta = 0.22$. We considered the compression ratio of $\alpha = 0.01$ and $N = 1000$ subcarriers.[6] Observe in Fig. 4 that the proposed scheme with truncated PA exhibited a performance loss over the optimal-PA counterpart. The performance gap increased upon increasing the SNR value, while it was not substantial in the low SNR regime, i.e., SNR < 10 dB.

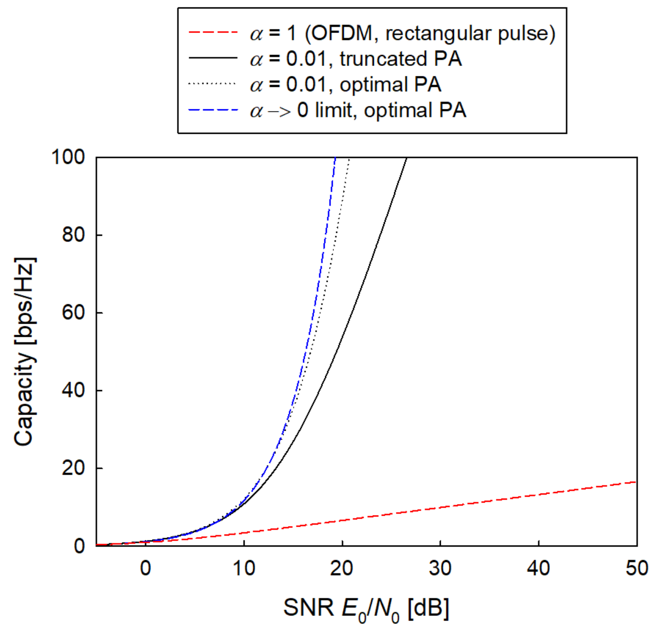

Fig. 4. Capacity of the proposed EVD-precoded NOFDM schemes with optimal and truncated PA, where the threshold for truncation was given by $t_h = 10^{-4}$, and the roll-off factor of an RRC shaping filter was set to $\beta = 0.22$. We considered the compression ratio of $\alpha = 0.01$ and $N = 1000$ subcarriers. The benchmark curve associated with the classic OFDM based on a rectangular pulse was also plotted.

Furthermore, in Fig. 5 we investigated the effects of the roll-off factor β on the capacity of the proposed EVD-precoded NOFDM scheme with truncated PA, where we considered the compression ratio of $\alpha = 0.01$, the threshold of $t_h = 10^{-4}$, and the $N = 1000$ number of subcarriers. Here, the roll-off factor of an RRC shaping filter was given by $\beta = 0.01, 0.22, 0.5,$ and 0.999. Observed in Fig. 5 that the capacity of the proposed scheme with truncated PA increased, upon decreasing the roll-off factor β.

Fig. 6 shows the calculated average power of transmit signals $\mathbb{E}[|x(t)|^2]$ in the proposed NOFDM scheme with optimal and truncated PA, which is designed to be unity in our model. The compression factor was varied from $\alpha = 0.01$ to 1, while the roll-off factor was set to $\beta = 0.22$. The threshold of the truncated PA scheme was given by $t_h = 10^{-8}, 10^{-7}, 10^{-6}$, and 10^{-4}. Observe in Fig. 6 that the truncated PA scheme with $t_h = 10^{-4}$ attained the accurate unity average power in

[6]The simulation parameters used in Fig. 4 corresponded to those of Fig. 2, except that the curves associated with relatively high α values (i.e., $\alpha = 0.5, 0.2, 0.1,$ and 0.05) were not shown in Fig. 4. This is because in a relatively high α value, all of the eigenvalues are typically higher than a threshold t_h. Hence, the truncation does not have to be activated in such a high-α scenario.

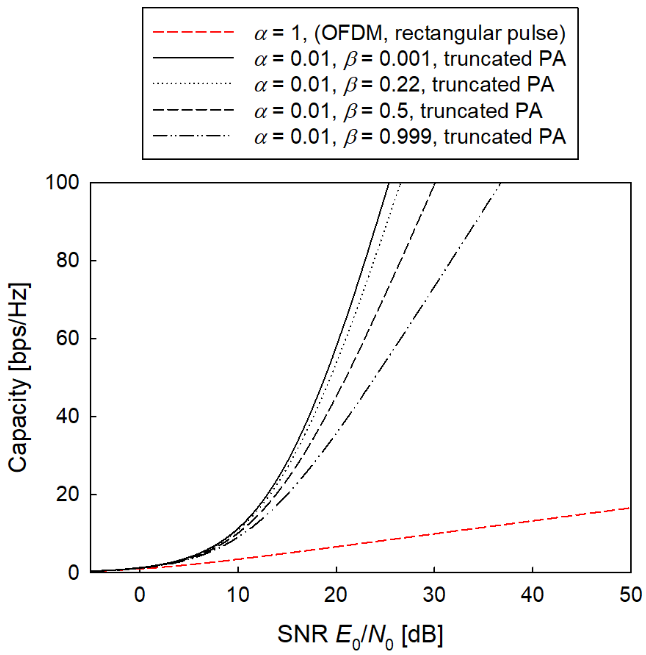

Fig. 5. Capacity of the proposed EVD-precoded NOFDM scheme with truncated PA, where the threshold for truncation was given by $t_h = 10^{-4}$, while considering the roll-off factor of $\beta = 0.01, 0.22, 0.5$ and 0.999, the compression ratio of $\alpha = 0.01$, and $N = 1000$ subcarriers. The benchmark curve associated with the classic OFDM based on a rectangular pulse was also plotted.

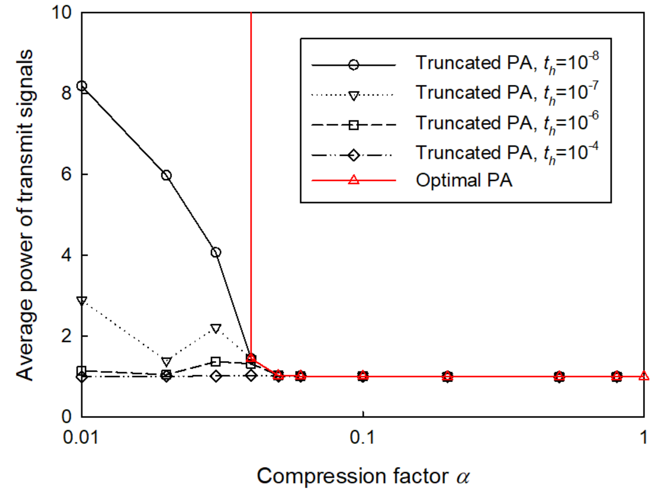

Fig. 6. The calculated average power of transmit signals $\mathbb{E}[|x(t)|^2]$ in the proposed NOFDM scheme with optimal and truncated PA, which is expected to be unity in our model. The compression factor was varied from $\alpha = 0.01$ to 1, while the threshold of the truncated PA scheme was given by $t_h = 10^{-8}, 10^{-7}, 10^{-6}$, and 10^{-4}. The roll-off factor was set to $\beta = 0.22$.

the entire τ range, since the significantly low eigenvalues were omitted for the generation of transmit signals. By contrast, for the scenarios of $t_h \leq 10^{-6}$ in the truncated PA scheme, the average transmit power became higher than unity when $\alpha < 0.05$, due to the unignorable errors in calculating the inverse of significantly low eigenvalues. Hence, the transmit signals were not correctly generated. Furthermore, in the optimal PA scheme, the average transmit power cannot be calculated in the wide compression-factor range of $\alpha < 0.04$. This is because as shown in Fig. 3, the part of the eigenvalues was too small to be tractable in the standard double-precision environment employed in our simulations.

VI. Effects of PSD and PAPR

As mentioned in Section IV, it is a challenging task to calculate significantly low eigenvalues, and inaccurate eigenvalues tend to cause the generation of inaccurate transmit signals $x(t)$. This tends to increase the PSD and the PAPR. Hence, in this section, we investigate the PSDs and the PAPRs in the proposed schemes.

A. PSD

Fig. 7(a) shows the PSDs of the conventional NOFDM scheme without PA, while Fig. 7(b) shows those of the proposed EVD-precoded NOFDM schemes with optimal and truncated PA. The benchmark curve of the classic OFDM using a rectangular pulse was also plotted. Note that the PSDs of the conventional EVD-precoded NOFDM scheme coincided with those of the conventional unprecoded NOFDM scheme in Fig. 7(a). The RRC shaping filter with a roll-off factor of $\beta = 0.22$ was employed for all the schemes, except for the classic OFDM scheme. The compression factor was given by $\alpha = 0.5, 0.2, 0.1, 0.08, 0.05, 0.04, 0.02$, and 0.01. The frame duration and the transmit energy were set to $T = 1$ and $E_0 = 1$, respectively. In order to calculate PSDs, each of the generated frames was sampled with the interval of $0.01T$. The threshold of our truncated PA was set to $t_h = 10^{-4}$. In Fig. 7(b), the PSDs of the proposed scheme with optimal PA are plotted for $\alpha \geq 0.05$, while those of the proposed scheme with truncated PA are plotted for $\alpha < 0.05$. This is because, in the proposed scheme with optimal PA, accurate transmit signals $x(t)$ cannot be generated in the low α regime, due to the effects of significantly low eigenvalues, as mentioned in Section IV. Additionally, the number of subcarriers was set to $N = N_{\rm OFDM}/\alpha = 10/\alpha$, such that the same total bandwidth was maintained to be approximately 10 [Hz], implying that the number of subcarriers of NOFDM was $1/\alpha$ times higher than that of OFDM. The simulation settings were considered for demonstrating that the proposed NOFDM signal is strictly band-limited.

Observe in Fig. 7(a) that the PSD of the conventional NOFDM scheme sharply dropped at the frequency of $[-5, 5]$ [Hz], regardless of the α value. A similar trend can be seen in the proposed scheme from Fig. 7(b); i.e., the PSDs of the proposed scheme with optimal PA ($\alpha \geq 0.05$), as well as those of the proposed scheme with truncated PA ($\alpha < 0.05$), were strictly bandlimited, as expected. Note that the spectral side-lobe level of the PSDs slightly increased upon decreasing α. Hence, the transmit signals of the proposed schemes are strictly bandlimited by appropriately introducing the truncated PA concept, depending on the α value.

Furthermore, Fig. 8 shows the PSDs of the proposed EVD-precoded NOFDM scheme with truncated PA, where the threshold was varied from $t_h = 10^{-4}$ to 0.1 while maintaining the compression factor of $\alpha = 0.01$. The other

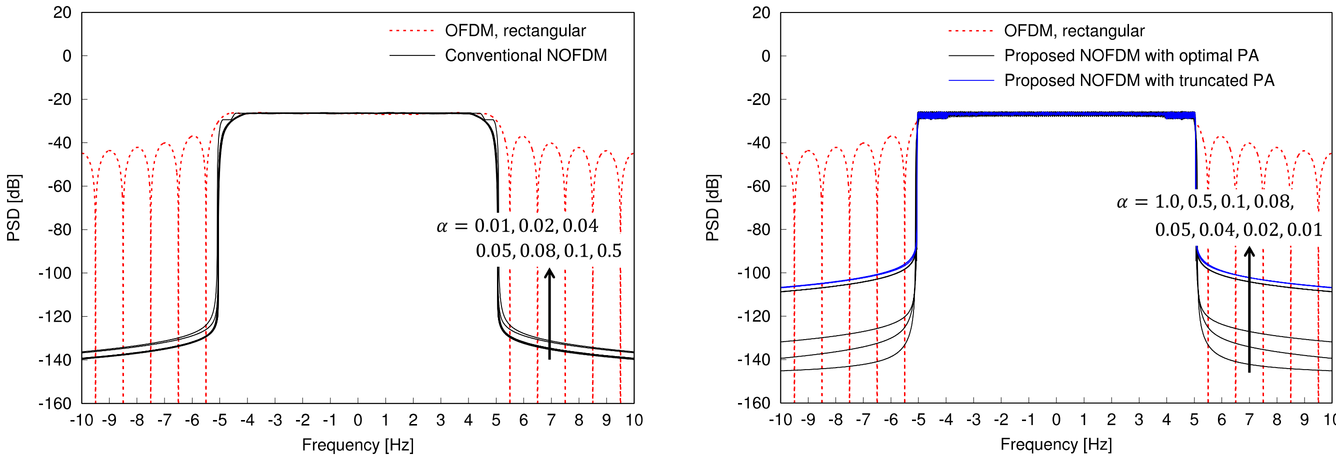

(a) Conventional EVD-precoded NOFDM

(b) Proposed EVD-precoded NOFDM

Fig. 7. PSDs of (a) the conventional EVD-precoded and unprecoded NOFDM schemes and (b) the proposed EVD-precoded NOFDM schemes with optimal and truncated PA. The number of subcarriers was set to $N = N_{\mathrm{OFDM}}\alpha = 10/\alpha$. The RRC filter with a roll-off factor of $\beta = 0.22$ was employed, and the compression factor was given by $\alpha = 1, 0.5, 0.2, 0.1, 0.08, 0.05, 0.04, 0.02$, and 0.01.

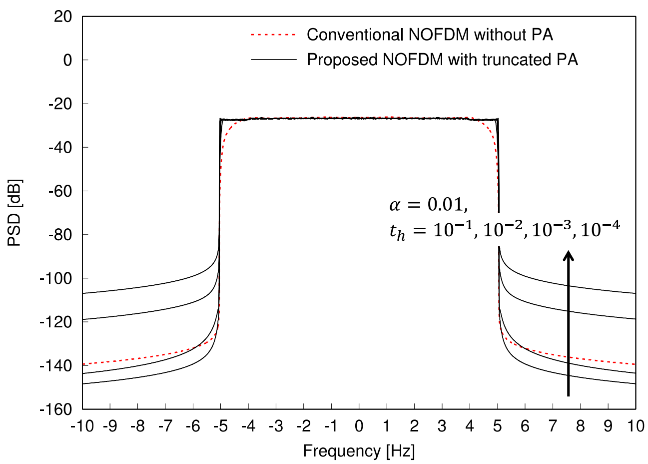

Fig. 8. PSDs of the proposed EVD-precoded NOFDM with truncated PA. The compression factor was fixed to $\alpha = 0.01$, while the threshold t_h was varied from 10^{-4} to 1.

system parameters are the same as those used in Fig. 7(b). For comparison, the PSD curve associated with the conventional NOFDM scheme ($\alpha = 0.01$) is also plotted. Observe in Fig. 8 that each PSD of the proposed scheme was cut off outside the bandwidth of [-5,5] [Hz]. Here, the spectral side-lobe level of the proposed scheme increased upon increasing the threshold t_h, although it remained sufficiently low in the simulated range, maintaining a lower level than that of the conventional NOFDM scheme.

In order to provide further insights, in Fig. 9, we plotted the PSDs of the NOFDM and OFDM signals, where the number of subcarrier was fixed to $N = 1000$. The RRC shaping filter with the roll-off factor of $\beta = 0.22$ was used for NOFDM, and the rectangular pulse was employed for OFDM. The compression factor of NOFDM was given by $\alpha = 0.5, 0.25, 0.125$ and 0.1 in Figs. 9(a), 9(b), 9(c), and 9(d), respectively, where all the N eigenvalues were used without truncation. Observe in Fig. 9 that in each α scenario, the total signal power of NOFDM was α (< 1) times that of OFDM.

B. PAPR

The PAPR is defined as the ratio of the maximum to the average power of the transmitted signals as follows: [33]

$$\zeta = \frac{\max |x(t)|^2}{\mathbb{E}\left[|x(t)|^2\right]}, \tag{94}$$

where $\max |x(t)|^2$ denotes the peak power of the transmitted signals in each frame, and $\mathbb{E}[|x(t)|^2]$ represents the average power.

Fig. 10 compares the complementary cumulative distribution functions (CCFD) of the PAPR in the proposed NOFDM schemes with optimal and truncated PA and the conventional NOFDM scheme without PA, where the roll-off factor was set to $\beta = 0.22$, while the compression factor was given by $\alpha = 1.0, 0.5, 0.1, 0.05$, and 0.01. The QPSK modulation was considered for all the schemes. In order to avoid the effects of significantly low eigenvalues emerged in the proposed NOFDM scheme, the proposed scheme with truncated PA, employing the threshold of $t_h = 10^{-4}$ was considered only for $\alpha = 0.01$. Furthermore, the number of subcarriers was given by $N_{\mathrm{OFDM}} = N\alpha = 100$, and hence we had the same bandwidth and average power for all the schemes. Let us observe in Fig. 10 that the proposed scheme tended to exhibit a higher PAPR than the conventional NOFDM scheme without PA and the classical OFDM scheme using a rectangular pulse, where the gap between the proposed and other benchmark schemes was lower than 0.4 dB for $\alpha = 0.5$. Upon decreasing the α value, the performance loss increased. Hence, the slightly high PAPR of the proposed scheme was at the cost of achieving a higher information rate than other benchmark schemes.

VII. BER Results

In this section, we provide our BER performance results based on Monte Carlo simulations, in order to numerically verify the capacity results of Section IV. We considered a

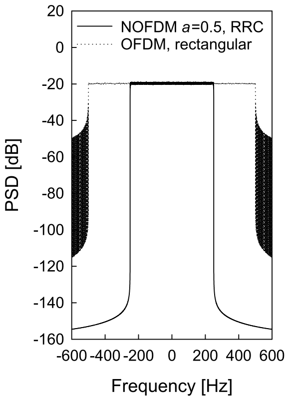

(a) $\alpha = 0.5$

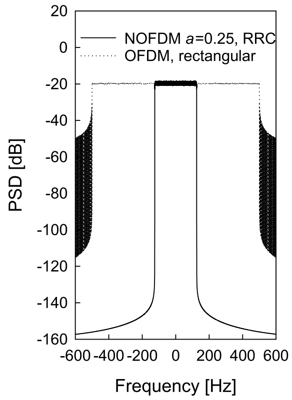

(b) $\alpha = 0.25$

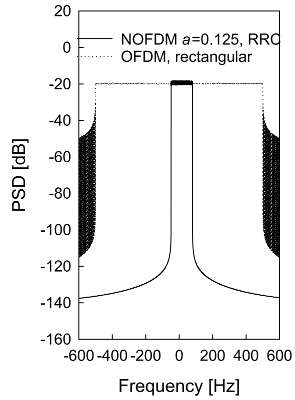

(c) $\alpha = 0.125$

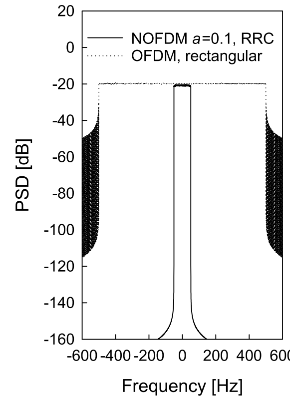

(d) $\alpha = 0.1$

Fig. 9. The PSD comparisons between NOFDM and OFDM, where the number of subcarrier was fixed to $N = 1000$. The RRC shaping filter with the roll-off factor of $\beta = 0.22$ was used for NOFDM, and the rectangular pulse was employed for OFDM. (a) $\alpha = 0.5$, (b) $\alpha = 0.25$, (c) $\alpha = 0.125$, and (d) $\alpha = 0.1$.

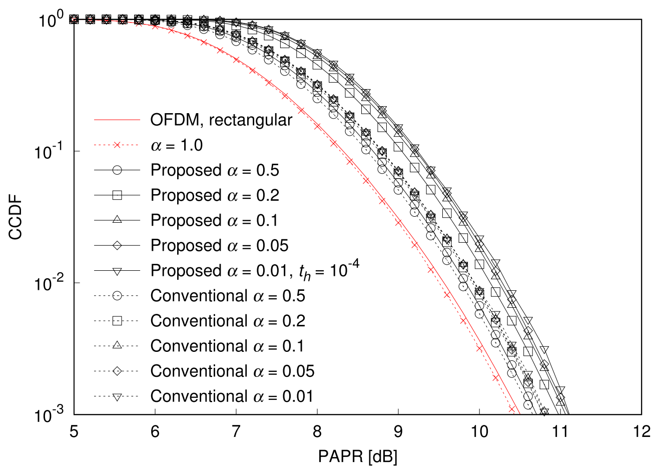

Fig. 10. PAPRs of the proposed EVD-precoded NOFDM schemes with optimal and truncated PA and the conventional NOFDM scheme without PA, where the number of subcarriers was given by $N_{\mathrm{OFDM}} = N\alpha = 100$, while employing QPSK for all the schemes. The compression factor was set to $\alpha = 0.5, 0.2, 0.1, 0.05$, and 0.01, and the roll-off factor of an RRC shaping filter was given by $\beta = 0.22$. The benchmark curve associated with the classic OFDM based on a rectangular pulse was also plotted.

three-stage serially concatenated turbo-coded architecture [36], which is portrayed in Fig. 11. At the transmitter, information bits are encoded by a half-rate recursive systematic coding (RSC) encoder, and the RSC-encoded bits are interleaved by an outer interleaver Π_1. Then, the interleaved bits are encoded by the unity-rate coding (URC) encoder. Furthermore, the URC-encoded bits are interleaved again by an inner interleaver Π_2, in order to obtain channel-encoded bits. The same near-capacity three-stage turbo architecture was also employed for the conventional NOFDM and OFDM benchmark schemes.

At the receiver, extrinsic information in the form of log-likelihood ratios (LLRs) is exchanged between the three soft decoders, i.e., the LLR calculator, URC decoder, and RSC decoder. The number of inner iterations and that of outer iterations are denoted I_{in} and I_{out}, respectively.

In our simulations, the number of subcarriers in NOFDM was maintained as $N = 1000$, and the interleaver length was given by 20000. Therefore, a total of 20000 channel-encoded bits were transmitted by 20 NOFDM frames in each Monte Carlo simulation. As mentioned, in this paper, the effects of inter-frame interference were ignored, such that $\epsilon = 0$. The number of inner iterations and that of outer iterations were set to $I_{\mathrm{in}} = 2$ and $I_{\mathrm{out}} = 40$, respectively.[7] Moreover, the normalized transmission rate R is calculated by

$$R = \frac{1}{2} \cdot \frac{\sum_{i=0}^{N-1} R_i}{(N-1)\alpha + (1+\beta+\epsilon)} \text{ [bps/Hz]}, \tag{95}$$

where R_i denotes the bit rate of the ith subcarrier. Note that the bit rate associated with the truncated subcarrier becomes $R_i = 0$. Furthermore, under the condition of $N\alpha \gg 1$, R is approximated by

$$R \simeq \frac{1}{2} \cdot \frac{\sum_{i=0}^{N-1} R_i}{N\alpha} \text{ [bps/Hz]}. \tag{96}$$

Fig. 12 compares the BERs of the proposed EVD-precoded NOFDM scheme with optimal PA and the conventional EVD-precoded NOFDM scheme without PA, each employing BPSK, where the roll-off factor of an RRC filter was given by $\beta = 0.22$. The compression factor was set to $\alpha = 0.5, 0.25, 0.125$, and 0.1, which corresponded to normalized transmission rates of $R = 1.00, 1.99, 3.97$, and 4.94 bps/Hz, respectively. For comparison, we also plotted the BER curves of the classical OFDM benchmark schemes with a rectangular pulse and an RRC-shaped pulse, employing QPSK, 16-QAM, 256-QAM, and 1024-QAM, which exhibited the rates similar to those of the proposed and conventional NOFDM schemes, i.e., $R = 1.00, 2.00, 4.00$, and 5.00 bps/Hz. Also, the SNRs associated with the capacities of the three schemes were included, which were calculated from 2(a) and 2(b). Since the eigenvalues were sufficiently high in the simulated range of $0.1 \leq \alpha \leq 0.5$, truncation does not have to be activated in the proposed scheme. Moreover, given an SNR E_0/N_0, the transmit power of the NOFDM scheme was 2, 4, 8, and 10 times

[7]In our extensive simulations, it was confirmed that the iterations of $I_{\mathrm{in}} = 2$ and $I_{\mathrm{out}} = 40$ were sufficiently high, and any substantial performance improvement may not be attained with further increase of $(I_{\mathrm{in}}, I_{\mathrm{out}})$.

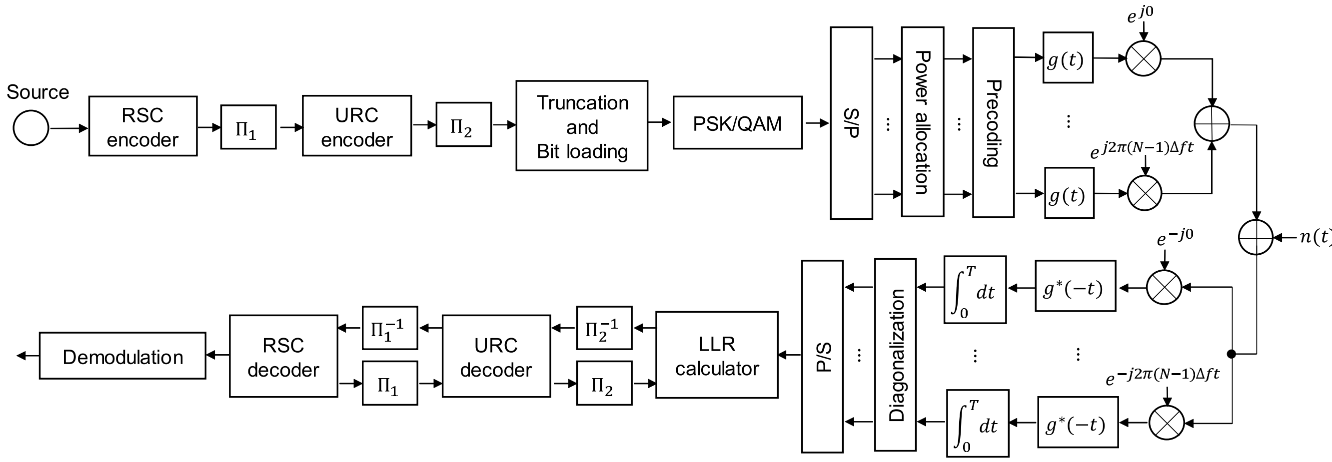

Fig. 11. Transceiver architecture of the proposed three-stage-concatenated turbo-coded EVD-precoded NOFDM with truncated PA.

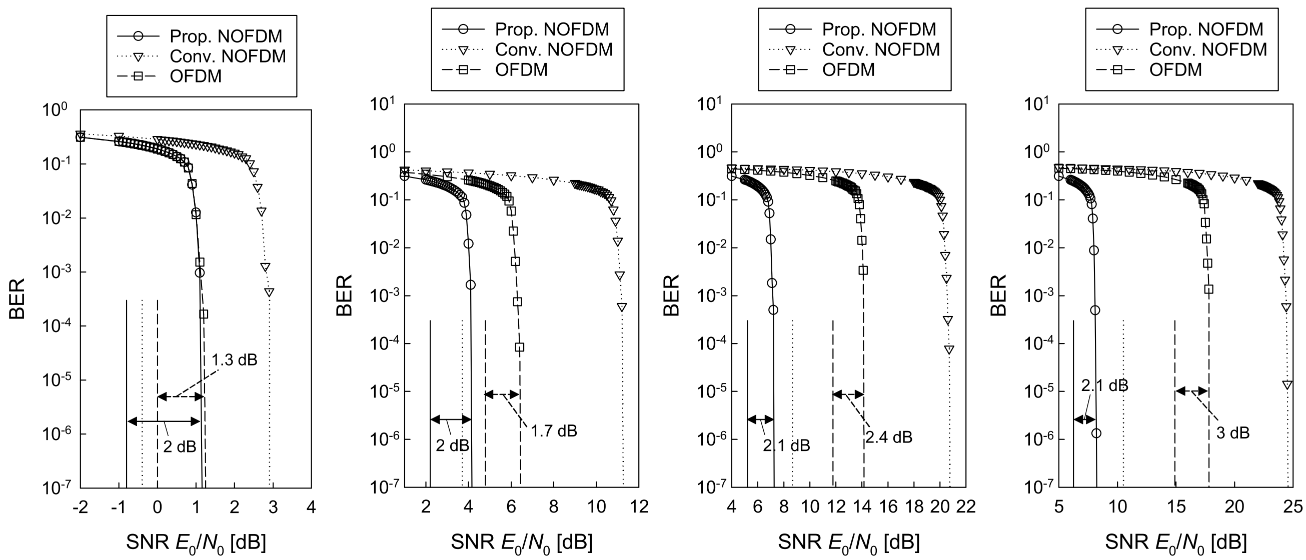

(a) 1 bps/Hz (b) 2 bps/Hz (c) 4 bps/Hz (d) 5 bps/Hz

Fig. 12. BER comparisons of the proposed EVD-precoded NOFDM scheme with optimal PA, the conventional EVD-precoded NOFDM scheme without PA, and the classical OFDM, each employing the three-stage-concatenated turbo-coded architecture. The compression factor was set to $\alpha = 0.5, 0.25, 0.125$, and 0.1, while maintaining the roll-off factor of $\beta = 0.22$. The proposed and the conventional NOFDM schemes employed BPSK, while the OFDM employed QPSK, 16-QAM, 256-QAM, and 1024-QAM. The target rates are given by (a) 1 bps/Hz, (b) 2 bps/Hz, (c) 4 bps/Hz, (d) 5 bps/Hz.

lower than that of the OFDM benchmark in Figs. 12(a), 12(b), 12(c), and 12(d), respectively. A further note is that the PSDs of NOFDM and OFDM in the scenarios of Figs. 12(a), 12(b), 12(c), and 12(d) corresponded to those of Figs. 9(a), 9(b), 9(c), and 9(d), respectively. Observe in Fig. 12 that the proposed scheme outperformed the conventional NOFDM and the OFDM schemes for $R \geq 2$ bps/Hz, as expected from the capacity results (Figs. 2(a) and 2(b)). The performance gain increased upon increasing the transmission rate. By contrast, the conventional EVD-precoded NOFDM scheme failed to outperform the OFDM benchmark for each R scenario. This is caused by the detrimental effects of low channel gains associated with low eigenvalues. Note that in Fig. 12 both the proposed NOFDM and the conventional OFDM schemes exhibited the near-capacity performance, where the BER cliffs were seen close to the associated capacity bounds. Hence, the performance advantage of the proposed NOFDM remains unchanged even if the OFDM attained further performance improvement by optimizing the channel-coding and modulation schemes.

Fig. 13 shows the BERs of the proposed EVD-precoded NOFDM with truncated PA in the ultra-dense subcarrier scenario of $\alpha = 0.01$, while varying the roll-off factor of an RRC shaping filter as $\beta = 0.01, 0.22, 0.5$, and 0.999. Here, the constellation sizes used for substreams were adapted in each β scenario. The threshold was given by $t_h = 10^{-4}$. More specifically, the normalized transmission rates were $R = 45.49, 44.60, 43.52$, and 41.70 bps/Hz for $\beta = 0.001, 0.22, 0.5$, and 0.999, where the ratios of activated substreams were $M/N = 30.3\%, 27.0\%, 20.2\%$, an 14.3%,

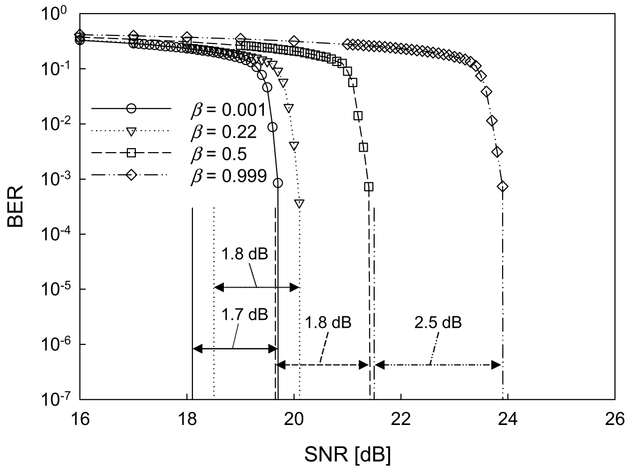

Fig. 13. BER performances of the proposed EVD-precoded NOFDM with truncated PA, where the roll-off factor was set to $\beta = 0.001, 0.22, 0.5$, and 0.999. Here, the compression factor was maintained as $\alpha = 0.01$, and the threshold was set to $t_h = 10^{-4}$.

respectively. Hence, in the simulated scenarios, the lower the roll-off factor β, the better the achievable BER performance. Additionally, the associated capacity limits were plotted, according to Fig. 5. It is observed in Fig. 13 that the gaps between the error-free SNRs and the associated capacity limits were lower than 2 dB, for $\beta = 0.001, 0.22$, and 0.5.

In this paper, we focused our attention on the investigations of the achievable bound of the NOFDM scheme. To provide further insights, the proposed NOFDM scheme faces several challenges and open issues as follows. In this paper, we assumed the AWGN channel for simplicity. This assumption allows us to carry out the eigenvalue decomposition of ICI matrix offline. However, in a realistic frequency-selective fading channel, the results of the eigenvalue decomposition has to be updated every channel's coherence time. Furthermore, the associated calculation complexity is significantly high, especially for a high number of subcarriers N. Next, in the NOFDM scheme, the sampling rate at the receiver is $1/\alpha$ (≥ 1) times higher than in the OFDM counterpart. Such a high sampling rate may not be intractable in the current technology, especially for a low-α and broadband scenario. Also, in the proposed NOFDM scheme with truncation, the threshold that truncates a significantly low eigenvalues depends on the calculation precision. Hence, there is a tradeoff between the achievable performance and the calculation precision, similar to precoded FTN signaling [37].

VIII. Conclusion

In this paper, we have proposed EVD-precoded NOFDM with optimal and truncated PA. Based on the eigenvalue-decomposed independent parallel substreams, the capacities of the conventional and proposed EVD-precoded NOFDM schemes were derived as extensions of the classical capacity of the OFDM counterpart. The derived capacities were used for optimizing the PA coefficients of the proposed scheme. Our theoretical analysis showed that the proposed scheme achieves higher performance than the conventional NOFDM scheme and the classical OFDM. To eliminate the limitations imposed by significantly low eigenvalues on our optimal PA, we introduced the concept of truncated PA into our scheme. Numerical simulation results demonstrated that the proposed schemes outperformed the conventional scheme and OFDM, without imposing any substantial spectrum broadening or any excessive PAPR increase.

References

[1] S. Osaki, T. Ishihara, and S. Sugiura, "Non-orthogonal frequency-division multiplexing based on eigenvalue decomposition," in *Proc. IEEE Veh. Technol. Conf. (VTC-Fall)*, Oct. 2020, pp. 1–5.

[2] J. B. Anderson, F. Rusek, and V. Öwall, "Faster-than-Nyquist signaling," *Proc. IEEE*, vol. 101, no. 8, pp. 1817–1830, Aug. 2013.

[3] I. Kanaras, A. Chorti, M. R. D. Rodrigues, and I. Darwazeh, "Spectrally efficient FDM signals: Bandwidth gain at the expense of receiver complexity," in *Proc. IEEE Int. Conf. Commun.*, Dresden, Germany, Jun. 2009, pp. 1–6.

[4] I. Darwazeh, H. Ghannam, and T. Xu, "The first 15 years of SEFDM: A brief survey," in *Proc. 11th Int. Symp. Commun. Syst., Netw. Digit. Signal Process. (CSNDSP)*, Budapest, Hungary, Jul. 2018, pp. 1–7.

[5] L. Dai, B. Wang, Y. Yuan, S. Han, C.-L. I, and Z. Wang, "Non-orthogonal multiple access for 5G: Solutions, challenges, opportunities, and future research trends," *IEEE Commun. Mag.*, vol. 53, no. 9, pp. 74–81, Sep. 2015.

[6] W. Kozek and A. F. Molisch, "Nonorthogonal pulseshapes for multicarrier communications in doubly dispersive channels," *IEEE J. Sel. Areas Commun.*, vol. 16, no. 8, pp. 1579–1589, Oct. 1998.

[7] A. Kliks, H. Bogucka, I. Stupia, and V. Lottici, "A pragmatic bit and power allocation algorithm for NOFDM signalling," in *Proc. IEEE Wireless Commun. Netw. Conf.*, Budapest, Hungary, Apr. 2009, pp. 1–6.

[8] G. Fettweis, M. Krondorf, and S. Bittner, "GFDM–Generalized frequency division multiplexing," in *Proc. VTC Spring - IEEE 69th Veh. Technol. Conf.*, Barcelona, Spain, Apr. 2009, pp. 1–4.

[9] N. Michailow *et al.*, "Generalized frequency division multiplexing for 5th generation cellular networks," *IEEE Trans. Commun.*, vol. 62, no. 9, pp. 3045–3061, Sep. 2014.

[10] S. Isam, I. Kanaras, and I. Darwazeh, "A truncated SVD approach for fixed complexity spectrally efficient FDM receivers," in *Proc. IEEE Wireless Commun. Netw. Conf.*, Mar. 2011, pp. 1584–1589.

[11] I. Darwazeh, T. Xu, T. Gui, Y. Bao, and Z. Li, "Optical SEFDM system; bandwidth saving using non-orthogonal sub-carriers," *IEEE Photon. Technol. Lett.*, vol. 26, no. 4, pp. 352–355, Feb. 15, 2014.

[12] S. V. Zavjalov, S. V. Volvenko, and S. B. Makarov, "A method for increasing the spectral and energy efficiency SEFDM signals," *IEEE Commun. Lett.*, vol. 20, no. 12, pp. 2382–2385, Dec. 2016.

[13] T. Xu and I. Darwazeh, "Transmission experiment of bandwidth compressed carrier aggregation in a realistic fading channel," *IEEE Trans. Veh. Technol.*, vol. 66, no. 5, pp. 4087–4097, May 2017.

[14] M. Nakao and S. Sugiura, "Spectrally efficient frequency division multiplexing with index-modulated non-orthogonal subcarriers," *IEEE Wireless Commun. Lett.*, vol. 8, no. 1, pp. 233–236, Feb. 2019.

[15] S. Osaki, M. Nakao, T. Ishihara, and S. Sugiura, "Differentially modulated spectrally efficient frequency-division multiplexing," *IEEE Signal Process. Lett.*, vol. 26, no. 7, pp. 1046–1050, Jul. 2019.

[16] L. Hanzo, M. Münster, B. Choi, and T. Keller, *OFDM and MC-CDMA for Broadband Multi-User Communications, WLANs and Broadcasting*. Hoboken, NJ, USA: Wiley, 2003.

[17] J. Huang, Q. Sui, Z. Li, and F. Ji, "Experimental demonstration of 16-QAM DD-SEFDM with cascaded BPSK iterative detection," *IEEE Photon. J.*, vol. 8, no. 3, pp. 1–9, Jun. 2016.

[18] Z. Li *et al.*, "Beyond 100 Gb/s SEFDM signal IM/DD transmission utilizing TDE with 20% bandwidth compression," *IEEE Commun. Lett.*, vol. 23, no. 11, pp. 2017–2021, Nov. 2019.

[19] Y. Wang *et al.*, "Efficient MMSE-SQRD-Based MIMO decoder for SEFDM-based 2.4-Gb/s-Spectrum-Compressed WDM VLC system," *IEEE Photon. J.*, vol. 8, no. 4, pp. 1–9, Aug. 2016.

[20] H. Ghannam, D. Nopchinda, M. Gavell, H. Zirath, and I. Darwazeh, "Experimental demonstration of spectrally efficient frequency division multiplexing transmissions at E-Band," *IEEE Trans. Microw. Theory Techn.*, vol. 67, no. 5, pp. 1911–1923, May 2019.

[21] S. Isam and I. Darwazeh, "Precoded spectrally efficient FDM system," in *Proc. 21st Annu. IEEE Int. Symp. Pers., Indoor Mobile Radio Commun.*, Sep. 2010, pp. 99–104.

[22] D. Rainnie, Y. Feng, and J. Bajcsy, "On capacity merits of spectrally efficient FDM," in *Proc. MILCOM - IEEE Mil. Commun. Conf.*, Tampa, FL, USA, Oct. 2015, pp. 581–586.

[23] J. Salz, "Optimum mean-square decision feedback equalization," *Bell Syst. Tech. J.*, vol. 52, no. 8, pp. 1341–1373, Oct. 1973.

[24] J. E. Mazo, "Faster-Than-Nyquist signaling," *Bell Syst. Tech. J.*, vol. 54, no. 8, pp. 1451–1462, Oct. 1975.

[25] D. Dasalukunte, F. Rusek, and V. Owall, "Multicarrier Faster-Than-Nyquist transceivers: Hardware architecture and performance analysis," *IEEE Trans. Circuits Syst. I, Reg. Papers*, vol. 58, no. 4, pp. 827–838, Apr. 2011.

[26] F. Schaich and T. Wild, "A reduced complexity receiver for multi-carrier faster-than-Nyquist signaling," in *Proc. IEEE Globecom Workshops (GC Wkshps)*, Dec. 2013, pp. 235–240.

[27] J. Zhou, Y. Qiao, Z. Yang, and E. Sun, "Faster-than-Nyquist non-orthogonal frequency-division multiplexing based on fractional Hartley transform," *Opt. Lett.*, vol. 41, no. 19, pp. 4488–4491, Oct. 2016.

[28] F. Rusek and J. Anderson, "Non binary and precoded faster than nyquist signaling," *IEEE Trans. Commun.*, vol. 56, no. 5, pp. 808–817, May 2008.

[29] F. Rusek and J. B. Anderson, "Constrained capacities for Faster-Than-Nyquist signaling," *IEEE Trans. Inf. Theory*, vol. 55, no. 2, pp. 764–775, Feb. 2009.

[30] T. Ishihara and S. Sugiura, "SVD-precoded Faster-Than-Nyquist signaling with optimal and truncated power allocation," *IEEE Trans. Wireless Commun.*, vol. 18, no. 12, pp. 5909–5923, Dec. 2019.

[31] Y. Feng, Y. Ma, Z. Li, C. Yan, and N. Wu, "Low-complexity factor graph-based iterative detection for RRC-SEFDM signals," in *Proc. 10th Int. Conf. Wireless Commun. Signal Process. (WCSP)*, Oct. 2018, pp. 1–6.

[32] B. Farhang-Boroujeny, "OFDM versus filter bank multicarrier," *IEEE Signal Process. Mag.*, vol. 28, no. 3, pp. 92–112, May 2011.

[33] A. Goldsmith, *Wireless Communications*. Cambridge, U.K.: Cambridge Univ. Press, 2005.

[34] T. M. Cover and J. A. Thomas, *Elements of Information Theory*. New York, NY, USA: Wiley, 1991.

[35] J. M. Varah, "The prolate matrix," *Linear Algebra its Appl.*, vol. 187, pp. 269–278, Jul. 1993.

[36] S. Sugiura, S. Chen, and L. Hanzo, "Coherent and differential space-time shift keying: A dispersion matrix approach," *IEEE Trans. Commun.*, vol. 58, no. 11, pp. 3219–3230, Nov. 2010.

[37] K. Masaki, T. Ishihara, and S. Sugiura, "Effects of eigenvalue distribution on precoded faster-than-Nyquist signaling with power allocation," in *Proc. IEEE Veh. Technol. Conf. (VTC-Fall)*, Oct. 2020, pp. 1–5.

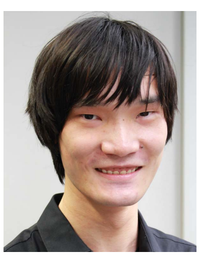

Seichiroh Osaki (Student Member, IEEE) received the B.E. degree in computer and information sciences from the Tokyo University of Agriculture and Technology, Japan, in 2019, where he is currently pursuing the master's degree. His research interest includes non-orthogonal multicarrier transmission.

Takumi Ishihara (Member, IEEE) received the B.E., M.E., and Ph.D. degrees in computer and information sciences from the Tokyo University of Agriculture and Technology, Japan, in 2016, 2017, and 2020, respectively.

He is currently a Post-Doctoral Research Fellow with the Institute of Industrial Science, The University of Tokyo, Tokyo, Japan. His research interest includes faster-than-Nyquist signaling. He was a recipient of the Yasujiro Niwa Outstanding Paper Award in 2019 and the 33rd Telecom System Technology Award (Honorable Mention) from the Telecommunications Advancement Foundation in 2018.

Shinya Sugiura (Senior Member, IEEE) received the B.S. and M.S. degrees in aeronautics and astronautics from Kyoto University, Kyoto, Japan, in 2002 and 2004, respectively, and the Ph.D. degree in electronics and electrical engineering from the University of Southampton, Southampton, U.K., in 2010.

From 2004 to 2012, he was a Research Scientist with Toyota Central Research and Development Laboratories, Inc., Nagakute, Japan. From 2013 to 2018, he was an Associate Professor with the Department of Computer and Information Sciences, Tokyo University of Agriculture and Technology, Tokyo, Japan. Since 2018, he has been an Associate Professor with the Institute of Industrial Science, The University of Tokyo, Tokyo, where he heads the Wireless Communications Research Group. He has authored or coauthored over 70 IEEE journal articles. His research has covered a range of areas in wireless communications, networking, signal processing, and antenna technology.

Dr. Sugiura was a recipient of numerous awards, including the Fifth Yasuharu Suematsu Award in 2019, the 33rd Telecom System Technology Award (Honorable Mention) from the Telecommunications Advancement Foundation in 2018, the Sixth RIEC Award from the Foundation for the Promotion of Electrical Communication in 2016, the Young Scientists' Prize by the Minister of Education, Culture, Sports, Science and Technology of Japan in 2016, the 14th Funai Information Technology Award (First Prize) from the Funai Foundation in 2015, the 28th Telecom System Technology Award from the Telecommunications Advancement Foundation in 2013, the Sixth IEEE Communications Society Asia-Pacific Outstanding Young Researcher Award in 2011, the 13th Ericsson Young Scientist Award in 2011, and the 2008 IEEE Antennas and Propagation Society Japan Chapter Young Engineer Award. He was also certified as an Exemplary Reviewer of the IEEE COMMUNICATIONS LETTERS in 2013 and 2014, and the IEEE TRANSACTIONS ON COMMUNICATIONS in 2018. He is currently serving as an Editor of the IEEE WIRELESS COMMUNICATIONS LETTERS.